Mechanics of Advanced Materials and Structures, 19(1-3):169–183, 2012.

Stiffness and Strength Prediction for Plain Weave Textile Reinforced Composites

Adi Adumitroaie[1] and E. J. Barbero[2]
Mechanical and Aerospace Engineering, West Virginia University,
Morgantown, WV 26506-6106, USA

Abstract

A model is presented to predict the mechanical hygro-thermo-elastic properties and strength values of composite materials reinforced with plain woven fabric. The laminate properties are calculated from basic constituents properties (fiber and matrix). A three-dimensional geometrical description of the reinforcing architecture is used. The local strain, stress, and constitutive property fields are evaluated under in-plane loading. Multiple modes of failure are monitored and stress redistribution due to progressive failure is evaluated using a novel approach. The model results are compared with experimental data.

Keywords

Fabric, Textile, Plain weave, Composite, Stiffness, Strength, Hygro-thermal.

1 Introduction

Woven fabric reinforcements are used in composites structures as an alternative to traditional unidirectional fiber reinforcing lay-ups, with applications in various fields such as automotive and aerospace engineering. The interest in this type of reinforcement has increased due to both the advances made in textile industry (the use of high performance fibers in high quality weaves), and the advantages conferred by the woven reinforcements compared to fiber lay-up (easier manipulation and lay-up during composite material manufacturing, good drapeability properties that allows the use of woven reinforcements in complex mold shapes, increased impact resistance and damage tolerance of the composite material). Along with these advantages, composite materials based on woven fabric reinforcements achieve high stiffness and strength, comparable with traditional fiber reinforcements.

A woven fabric is obtained by interlacing of individual tows. The textile industry offers a large variety of weaving styles, among which the plain weave is of great interest for structural applications. The plain weave belongs to the category of *2D* (featuring only in-plane laid tows, no through the thickness reinforcements), *biaxial* (the tows are along two in-plane directions), and *orthogonal* (the two tow directions are perpendicular) woven fabrics. The two sets of individual tows are called *warp* (along the longitudinal direction of the weaving machine) and *fill*. Yet, due to the inherent

[1]Graduate Research Assistant
[2]Corresponding author. The final publication is available at http://dx.doi.org/10.1080/15376494.2011.572245

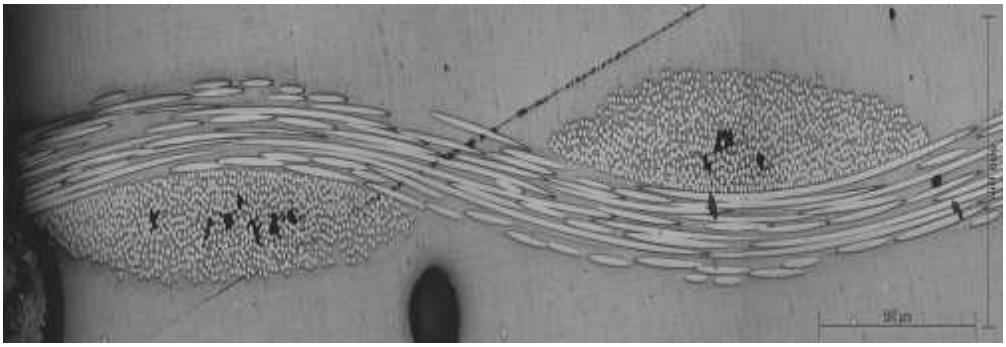

Figure 1: Photomicrograph of a textile-reinforced composite lamina. The undulation of the fill and the cross-section of the warp are shown.

undulation and cross-sectional shape of fill and warp tows, the plain weave reinforcement features a complex 3D structural behavior, which has to be taken into account.

Due to their applicability in high performance structures, woven fabric reinforced composite materials have been extensively studied, in order to proper understand their mechanical behavior, to tailor the desired material properties, to maximize their performances, and to wisely design structural parts based on this type of composites. Both numerical (FEA) and analytical methods have been proposed to study the mechanical behavior of woven fabric reinforced composites. While the numerical methods could provide more accurate results based on less modeling assumptions, they are difficult to generalize, one discretization applying to one singular case. Yet analytical models can provide a good level of accuracy (providing that the main features of the material behavior are preserved), and they are easier to use for parametric studies. The present study falls in the latter category.

The mosaic and the crimp models [1] are among the first analytical models that deal with plain weave reinforcement. The mosaic model does not consider the undulation and the continuity of individual tows. The crimp model takes this into account along only one direction (the direction of the unidirectional loading case, coinciding with the fill direction). Due to this simplified description, the mosaic and the crimp models are used only for the evaluation of stiffness properties. From the failure and strength analysis point of view, the crimp model is able to describe only the *knee* behavior under unidirectional loading (that is, the early stage of transverse warp failure). A complete and accurate stress analysis is not possible due to lack of complete description of the geometry of the reinforcement.

These first models are further developed in [2, 3], where double undulation along both fill and warp direction is considered. While in [2] the improved geometrical description is used to calculate the stiffness properties, the strength analysis in [3] is again performed by canceling the undulation along warp direction. This limits the use of the strength model to unidirectional loading case only.

An accurate description of the complex structure of the woven fabric reinforcement is made in [4, 5]. In this case, the gap in between adjacent fill and warp tows is not considered, and the failure analysis is based on Tsai-Wu stress failure criterion, which does not offer information about the mode of failure. In this way, it is not possible to differentiate between early failure modes such as transverse warp failure or shear failure under tensile loading, and final fiber failure.

A comprehensive description and analysis of the plain weave reinforced laminates is performed in [6–9], including the 3D geometry of the fabric reinforcement, the gap between tows, and material and geometrical nonlinearity. Two different ways of calculation are proposed in these references. The Cell Array Model (CAM) better preserves the geometrical description, and it is used for stiffness

calculation. Since CAM becomes difficult to handle for stress calculation, the Slice Array Model (SAM) is proposed in this case. To some extent, the SAM approximates the undulation of the tow transverse to the loading direction as a mean value. While the advanced features involved in these models are supposed to confer an increase in accuracy, they reduce at the same time the potential of the model to be developed for other weaving patterns, such us twill and satin. The problem of modeling the mechanical properties and behavior of more general twill and satin weaving patterns for the fabric reinforcement is approached in [10, 11].

The model proposed in this work calculates the hygro-thermo-elastic coefficients and the strength of plain weave reinforced laminates in a more general, systematic way with less simplifying approximations. The complex geometry of the reinforcement is described in detail and the gap between fill and warp tows is considered. Pointwise Classical Lamination Theory (CLT) in used to calculate the material properties and the complex stress state under loading. Multiple modes of failure are monitored, and stress redistribution during failure propagation is modeled. The model reaches a balance between complexity, accuracy and the possibility of further development (for example, to the case of biaxial loading or the case of other weaving patterns, such as twill and satin weaves).

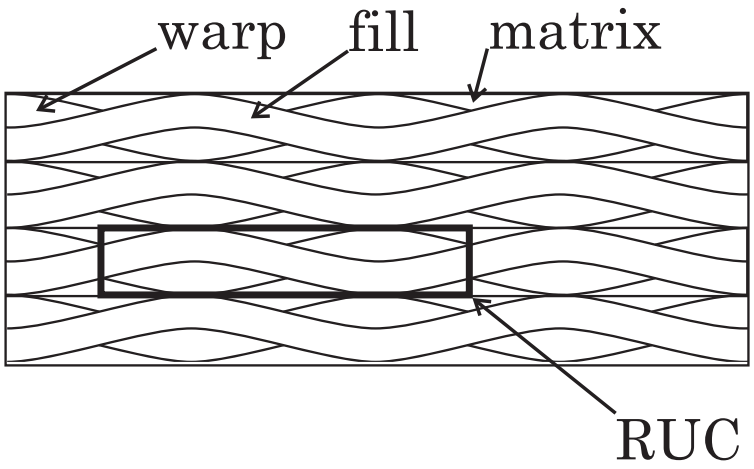

Figure 2: In-phase, textile-reinforced laminate.

2 Geometry and Materials

The main difference between woven fabric reinforcement and traditional unidirectional reinforced layers is, of course, the weaving (tows interlacing). The process of fibers (tows) layout by weaving confers advantages (Section 1) to composites based on this type of reinforcement, especially from the processing point of view, by easier handling and better drapeability on complex shaped molds. At the same time, the interlacing of tows changes the mechanical behavior of the composite material, due to the inherent undulation of fill and warp, as observed in Fig. 1, 2, 3. According to their degree of undulation (defined as the crimp level), the fill and warp tows does not behave as an unidirectional reinforcement, but rather as rotated, off-axis reinforcement. The rotation axis for the woven fill and warp tows is not the z axis, as in the case of off-axis unidirectional plies, but are the y and x axes, respectively (see Fig. 4). In this way, the woven fabric reinforcement gains a complex 3D characteristic that influences its final mechanical behavior.

Furthermore, as it can be observed in Fig. 2, the use of woven tows instead of unidirectional tapes as basic reinforcing elements confers a complex geometry to the composite material cross-

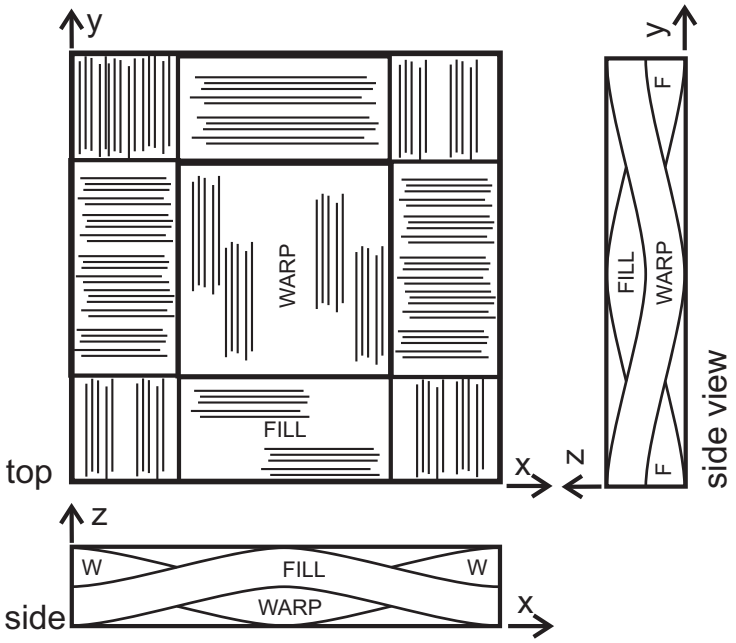

Figure 3: Repetitive Unit Cell (RUC) of a plain weave textile reinforced composite.

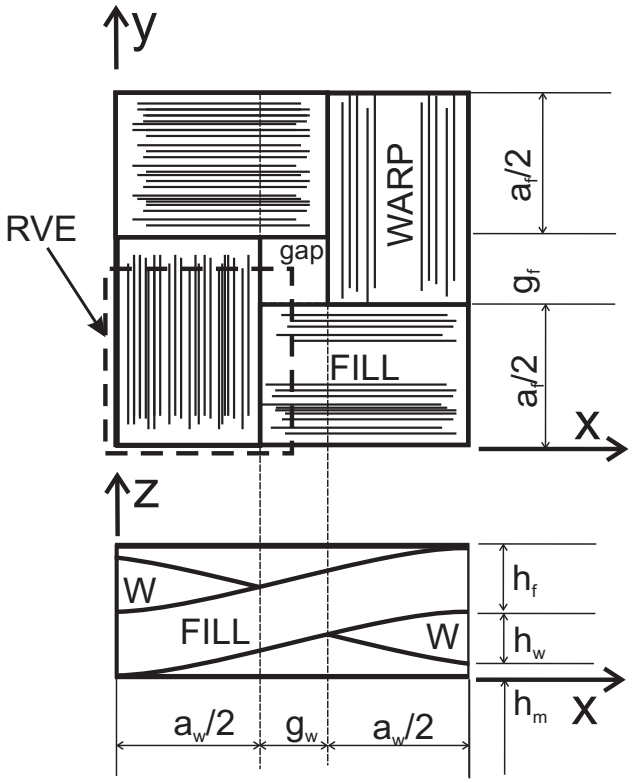

Figure 4: One-quarter RUC of a plain weave textile reinforced composite. Selection of Representaive Volume Element (RVE) for computation

section. Due to the weaving process, the tows have a lenticular shape of variable thickness, with pure matrix packages in between the interlacing points of fill and warp.

Another feature of the woven fabric reinforcements is the gap between two adjacent tows, g_f and g_w in Fig. 4. The presence and the dimension of the gap region might be an inherent result of the weaving process, or it might be an desired design parameter, which has an influence in both the dry fabric properties (for example, a given amount of gap improves the capacity of dry fabric to conform on complicated shapes during the manufacturing of complex composite perts), and the mechanical properties of the final composite material (for example, the bigger the gap region, the lower the elastic modulus of the fabric reinforced composite, as it can be seen latter).

All these elements of variable complex 3D geometry will have as result a variable stiffness field in the composite material, with further influence on the local strain-stress distribution inside of the material under external loading, which will be reflected in the mechanical properties of the composite material, as shown latter. Based on these observations, is is expected that an accurate geometry description of the woven reinforcement will play a role in the accuracy of the model output, this being the reason why the present model takes into account the tows undulation in both fill and warp directions.

Another advantage of this precise geometrical description is that this is the only way to precisely calculate the fiber volume fraction inside the individual fill and warp tows $V_f^{f,w}$, starting from the overall fiber volume fraction of the composite material V_f^0. The two are obviously different due to the presence of the pure matrix packages. While the latter is an input data for the model (experimentally determined from composite samples by acid digestion or burn-out methods [13, 14]), the former is a calculated parameter with direct influence on the thermo-elastic and strength properties of the composite tow, which are crucial to the properties of the fabric-reinforced composite lamina (or laminate). Accurate determination of the fiber volume fraction $V_f^{f,w}$ inside of fill and warp is essential for accurate predictions based on fiber and matrix properties.

The proposed model applies the method of the *Repetitive Unit Cell* (RUC), that is considered to be representative for the mechanical behavior of the lamina. The RUC is the smallest geometrical unit that describes all the features of the lamina. Once the mechanical properties of the RUC are modeled, these are considered to be representative for the composite material as a whole. For the case of plain weave reinforcement, considering the hypothesis of out-of-phase [2] or in-phase (Fig. 2) arrangement of the ply sequence over the laminate thickness, the RUC can be selected as in Fig. 3.

Furthermore, in order to reduce the computational effort, smaller units such as in Figure 4 can be selected for analysis, taking advantage of geometrical and material symmetry. Although the selected smaller unit is representative for the whole material properties and behavior, it does not feature repetitivity any more. Thus, the smaller unit used for analysis is regarder as *Representative Volume Element* (RVE) in the following. Selecting a smaller RVE facilitates easier computation. The smallest selection of RVE is marked with dashed line in Fig. 4, and it is detailed in Fig. 5.

Nesting of adjacent plies along z (thickness) direction of a multi-layered fabric reinforced laminate can take place during the manufacturing process of the composite material [15]. The nesting effect is neglected in the present model.

The input parameters for the model are (see Figure 4 and Table 1):

- the thickness of the fill and warp tows, and the thickness of the neat-matrix layer: h_f, h_w, h_m.
- the width of the fill and warp tows: a_f, a_w.
- the gap between adjacent fill and warp tows: g_f, g_w.

- the overall fiber volume fraction V_f^0

The most relevant way to consider these input parameters is to measure them by photomicrograph observation on material samples [16] (similar to Fig. 1). The present work relies on experimental measurements available in the literature [7, 12]. Therefore, it is assumed that the geometrical parameters reported are average values from a repetitive number of samples [7, 12]. During preliminary design, and lacking actual geometrical measurements, these parameters may be taken from measurements on dry fabric. Caution has to be paid to this practice, because all the above geometrical parameters may vary during manufacturing, due to the pressure applied on the fabric during vacuum bagging or resin transfer molding. The overall fiber volume fraction V_f^0 can be measured by acid digestion or burn-out [13, 14] or estimated from prior experience with similar reinforcements and manufacturing processes.

The proposed geometrical description makes use of the following trigonometric functions in order to completely describe the 3D geometry of the RVE. First, the z coordinate of the mid-plane of the undulated fill and warp tows (Fig. 4, 5) are described by

$$\begin{aligned} z_f(x) &= -\frac{h_f}{2} \cdot cos\frac{\pi x}{a_w + g_w} \quad \text{for} \quad y \in \left[0, \frac{a_f}{2}\right] \\ z_w(y) &= \frac{h_w}{2} \cdot cos\frac{\pi y}{a_f + g_f} \quad \text{for} \quad x \in \left[0, \frac{a_w}{2}\right] \end{aligned} \tag{1}$$

and the variable thickness of the tows cross-section (Fig. 4) by

$$\begin{aligned} e_f(y) &= |h_f \cdot cos\frac{\pi y}{a_f}| \quad \text{for} \quad y \in \left[0, \frac{a_f}{2}\right] \\ e_w(x) &= |h_w \cdot cos\frac{\pi x}{a_w}| \quad \text{for} \quad x \in \left[0, \frac{a_w}{2}\right] \end{aligned} \tag{2}$$

In this way, the top and bottom bounding surfaces of both fill and warp tows inside the RVE can be mathematically described as

$$\begin{aligned} z_f^{top}(x,y) &= z_f(x) + \frac{1}{2}\, e_f(y) \\ z_f^{bot}(x,y) &= z_f(x) - \frac{1}{2}\, e_f(y) \\ z_w^{top}(x,y) &= z_w(y) + \frac{1}{2}\, e_w(x) \\ z_w^{bot}(x,y) &= z_w(y) - \frac{1}{2}\, e_w(x) \end{aligned} \tag{3}$$

and the 3D geometrical description of the RVE is complete (see Fig. 5). Alternative geometry descriptions proposed in [2] (based on elliptical shape functions), and in [7] (based on corrected trigonometric shape functions) proved to be cumbersome for the general analysis case including gap and general in-plane loading.

After the 3D geometrical description of the RVE is complete, the following geometrical parameters can be calculated (see Fig. 5). The undulation angle (i.e., the local off-axis angles of fill and warp tows) are

$$\begin{aligned} \theta_f(x) &= \left| arctan\left(\frac{d}{dx} z_f(x)\right)\right| \\ \theta_w(y) &= \left| arctan\left(\frac{d}{dy} z_w(y)\right)\right| \end{aligned} \tag{4}$$

The cross-sectional area of the fill and warp tows are

$$A_f = \int_0^{a_f/2} e_f(y)dy = \frac{h_f a_f}{\pi}$$
$$A_w = \int_0^{a_w/2} e_w(x)dx = \frac{h_w a_w}{\pi} \tag{5}$$

The developed lengths of the undulated fill and warp tows inside of the RVE are

$$L_f = \int_0^{(a_w+g_w)/2} \sqrt{1+\left(\frac{d}{dx}z_f(x)\right)^2}\,dx$$
$$L_w = \int_0^{(a_f+g_f)/2} \sqrt{1+\left(\frac{d}{dy}z_w(y)\right)^2}\,dy \tag{6}$$

and the volumes occupied by the fill and warp tows inside of the RVE are

$$v_f = A_f\ L_f$$
$$v_w = A_w\ L_w \tag{7}$$

At this point, the crimp of the tow, which is an overall measure of the tow undulation defined by the ratio between the developed (straightened) length of the tow (6) and the length occupied by the tow inside of material, can be calculated as

$$c_f = \left(1 - \frac{a_w + g_w}{2L_f}\right) \cdot 100\ [\%]$$
$$c_w = \left(1 - \frac{a_f + g_f}{2L_w}\right) \cdot 100\ [\%] \tag{8}$$

Based on these parameters, and having the material overall fiber volume fraction V_f^0 as an input parameter , the fiber volume fraction inside the fill and warp tows can be calculated as

$$V_f^f = V_f^w = V_f^o \left(\frac{v_{RVE}}{v_f + v_w}\right) = V_f^o \frac{h(a_f + g_f)(a_w + g_w)}{4(v_f + v_w)} \tag{9}$$

In (9) it is assumed that $V_f^f = V_f^w$ in order to be able to compute the tow volume fraction from the known geometry of the fabric and the overall volume fraction V_f^o because the later is easily obtained by burn-out or acid digestions tests. The model presented herein does work with different values of V_f^f, and V_f^w, but to differentiate between V_f^f, and V_f^w, one would have to measure them in-situ. Therefore, for expedience, it is assumed that they are equal and provided by (9).

The results provided by the proposed model are validated against experimental results taken from literature [8,12]. Accordingly, the cases considered here use as input the overall fiber volume fraction V_f^0, and the geometrical parameters $h_{f,w}, a_{f,w}, g_{f,w}$ corresponding to those experimented samples [7,12] (see Table 1).

3 Hygro-Thermo-Elastic Properties

The hygro-thermo-elastic properties of the fabric reinforced composite are calculated starting with the properties of the basic constituents: transversely isotropic fibers and isotropic matrix.

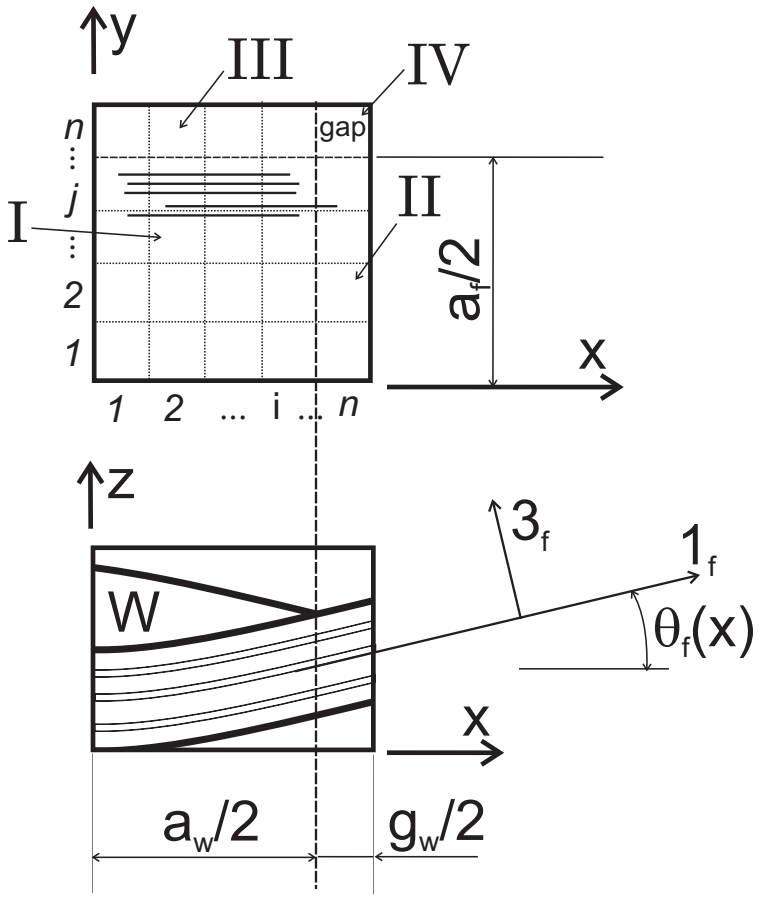

Figure 5: Plain weave RVE displaying the 2D mesh on the top surface.

Table 1: Geometrical parameters for several plain weave fabrics

	Tow width [mm]		Tow thickness [mm]		Gap [mm]		Matrix thickness [10^{-3}mm]	Fiber volume fraction Overall (exp.)	Tow (calc.)
#	a_f	a_w	h_f	h_w	g_f	g_w	h_m	V_f^o	$V_f^f = V_f^w$
1	0.45	0.45	0.048	0.048	0.30	0.30	2.0	0.23(*)	0.63
2	0.68	0.62	0.090	0.090	0.04	0.10	0.0	0.40	0.69
3	0.62	0.68	0.090	0.090	0.10	0.04	0.0	0.43	0.74
4	0.86	0.84	0.110	0.110	0.00	0.02	0.5	0.46	0.73
5	0.96	1.10	0.080	0.080	0.18	0.04	1.0	0.44	0.77

(*) outlier data point for sample #1.

The hygro-thermo-elastic and strength properties of the fiber and matrix constituents are taken from [6, 8]. Based on this, and considering the calculated tow fiber volume fraction $V_f^{f,w}$ (9), micromechanical models are used in order to calculate the hygro-thermo-elastic coefficients and strength values of individual fill and warp tows regarded as unidirectional fiber reinforced composites in their own $(1,2,3)_{f,w}$ material coordinate system (Fig. 5). For the case of elastic coefficients, the Periodic Microstructure Model [17,18] was used, while for the case of hygro-thermal coefficients and strength values, micro-mechanical models from [19], [**?**, p.3–20,21] and [21, p.51,52] were used.

Then, having calculated the local undulation angles $\theta_{f,w}(x,y)$ (4), the individual fill and warp tows are regarded as off-axis unidirectional reinforcements, as explained in Section 2. Thus, the local hygro-thermo-elastic properties of fill and warp tows can be calculated at any (x,y) location, corresponding to the $\theta_{f,w}(x,y)$ off-axis angle (Fig. 5) at that (x,y) location (see Appendix).

Next, each (x,y) location of the RVE is modeled with a matrix/fill/warp/matrix stacking sequence (Fig. 5). The computational effort is considerably increased if the model considers the gap between adjacent fill and warp tows, $g_{f,w}$. In this case, four different regions of the RVE with different stacking sequences have to be considered (Fig. 5). From the bottom of the laminate, the laminate stacking sequence (LSS) is matrix/fill/warp/matrix in region I; matrix/fill/matrix in region II; matrix/warp/matrix in region III; and only matrix in region IV, which is the gap. Based on the calculated local properties of fill and warp tows (Appendix), and using a point-wise CLT, the local hygro-thermo-elastic coefficients at any (x,y) location of the RVE can be calculated as

$$A_{i,j}(x,y), B_{i,j}(x,y), D_{i,j}(x,y) = \int_{-h/2}^{h/2} (1, z, z^2) \cdot \overline{Q}_{i,j}(x,y)\, dz \tag{10}$$

where $A_{i,j}(x,y), B_{i,j}(x,y), D_{i,j}(x,y) \quad (i,j = 1,2,6)$ are the RVE local stiffness coefficients, and

$$\begin{Bmatrix} N_x^T \\ N_y^T \\ N_{xy}^T \end{Bmatrix}(x,y), \begin{Bmatrix} M_x^T \\ M_y^T \\ M_{xy}^T \end{Bmatrix}(x,y) = \Delta T \int_{-h/2}^{h/2} (1,z) \cdot \left[\overline{Q}(x,y)\right] \cdot \begin{Bmatrix} \alpha_x(x,y) \\ \alpha_y(x,y) \\ \alpha_{xy}(x,y) \end{Bmatrix} dz$$
$$\begin{Bmatrix} N_x^M \\ N_y^M \\ N_{xy}^M \end{Bmatrix}(x,y), \begin{Bmatrix} M_x^M \\ M_y^M \\ M_{xy}^M \end{Bmatrix}(x,y) = \Delta m \int_{-h/2}^{h/2} (1,z) \cdot \left[\overline{Q}(x,y)\right] \cdot \begin{Bmatrix} \beta_x(x,y) \\ \beta_y(x,y) \\ \beta_{xy}(x,y) \end{Bmatrix} dz \tag{11}$$

where $\left\{N_x^{T,M}, N_y^{T,M}, N_{xy}^{T,M}\right\}(x,y), \left\{M_x^{T,M}, M_y^{T,M}, M_{xy}^{T,M}\right\}(x,y)$ are the induced thermal (superscript T) and moisture absorption (superscript M) distributed in-plane loads (forces and bending moments), at any (x,y) location of the RVE. The remaining parameters appearing in (10), (11) are defined in the Appendix.

At this point, the RVE is locally (i.e., at any (x,y) location) characterized by the field of local stiffness matrices $A(x,y)$, $B(x,y)$, $D(x,y)$, and the field of distributed in-plane induced loads $N^{T,M}(x,y)$, $M^{T,M}(x,y)$. In order to calculate the composite material properties, two instances of homogenization theory are invoked. These are the parallel/parallel (iso-strain/iso-strain) model [4,6,22] for the assemblage of local stiffness coefficients, and the series-parallel (iso-stress/iso-strain) model [22] for the assemblage of local induced loads. According with these two homogenization models, the global extensional stiffness coefficients can be calculated as

$$[A] = \frac{4}{(a_f + g_f)(a_w + g_w)} \int_0^{(a_w+g_w)/2} \int_0^{(a_f+g_f)/2} [A(x,y)] dx dy \tag{12}$$

Table 2: The calculated hygro-thermo-mechanical properties of fabric reinforced composite

	Modulus [GPa]			Poisson's ratio	Thermal expansion [$\mu\varepsilon$/C]		Moisture expansion [$10^{-3}\varepsilon$]		Strength Tensile [MPa]		Shear
#	E_x	E_y	G_{xy}	ν_{xy}	α_x	α_y	β_x	β_y	F_{xt}	F_{yt}	F_{xy}
1	13.02	12.02	2.57	0.18	23.75	23.75	91.26	91.26	275	275	36
2	19.68	18.87	3.86	0.17	16.80	17.64	51.16	54.30	310	310	38
3	20.61	21.46	4.47	0.17	16.16	15.43	47.83	45.10	335	335	38
4	22.12	21.89	4.56	0.17	15.25	15.44	42.73	43.40	325	325	38
5	48.94	54.45	4.73	0.06	5.44	4.60	21.11	18.67	415	415	106

and the global thermal and moisture absorption induced forces can be calculated as

$$\{N\}^{T,M} = \frac{4}{(a_f + g_f)(a_w + g_w)} \int_0^{(a_w+g_w)/2} \int_0^{(a_f+g_f)/2} \left\{N^{T,M}(x,y)\right\} dxdy \tag{13}$$

Based on these global parameters, the engineering moduli are calculated as [19, 22]

$$\begin{aligned} E_x &= (\alpha_{11} h)^{-1} \\ E_y &= (\alpha_{22} h)^{-1} \\ G_{xy} &= (\alpha_{66} h)^{-1} \\ \nu_{xy} &= -\frac{\alpha_{12}}{\alpha_{11}} \end{aligned} \tag{14}$$

where $[\alpha] = [A]^{-1}$ is the compliance matrix, and the thermal and moisture absorption expansion coefficients are calculated as [22]

$$\begin{Bmatrix} \alpha_x \\ \alpha_y \\ \alpha_{xy} \end{Bmatrix} = [A]^{-1} \cdot \begin{Bmatrix} N_x^T \\ N_y^T \\ N_{xy}^T \end{Bmatrix} \quad ; \quad \begin{Bmatrix} \beta_x \\ \beta_y \\ \beta_{xy} \end{Bmatrix} = [A]^{-1} \cdot \begin{Bmatrix} N_x^M \\ N_y^M \\ N_{xy}^M \end{Bmatrix} \tag{15}$$

The hygro-thermal-elastic coefficients calculated by the present model are listed in Table 2, and the comparison with experimental results [12] are presented in Table 3. Predicted values of E_x compare very well for samples #2–5 for which reliable values of overall fiber volume fraction are available (Table 1). The value of volume fraction for sample #1 reported in Table 1 is too low for the set. As a result, the predictions are off with respect to the measured response. Predicted values of G_{xy} compare very well with experimental values measured by the ±45 test. The 10^o test is not as well regarded as the ±45 test, or as ASTM D 5379; therefore, the 10^o test results do not agree well with either the ±45 results or the model predictions. Predicted values of thermal expansion coefficient α_x compare very well with experimental values measured by the dilatometer test but no so well when compared with strain-gage results, possibly due to deficiencies from that test procedure. Note that predictions for sample #1 are always suspect because of the outlier data of overall fiber volume fraction reported in Table 1.

Using the current analytical modeling approach, a parametric study can be performed with respect to the input weaving parameters $a_{f,w}, h_{f,w}, g_{f,w}$. These parameters can be controlled during

Table 3: Comparison of predicted and experimental [12] thermo-elastic properties.

	E_x [GPa]		[%]		G_{xy} [GPa]			ν_{xy}		α_x [$\mu\varepsilon/C$]		
#	Calc.	Exp.	SD	error	Calc.	Exp. $[10^o]_T$	Exp. $[\pm 45^o]_T$	Calc.	Exp.	Calc.	Exp. SG	Exp DM
1	13.02	20.0	0.8	34.88	2.57	6.25	2.94	0.18	-	23.75	19.58	19.51
2	19.68	21.5	1.0	8.64	3.86	6.89	3.57	0.17	-	16.80	13.69	15.45
3	20.61	20.8	0.7	0.91	4.47	-	-	0.17	-	16.16	-	-
4	22.19	22.8	1.2	2.99	4.56	8.33	5.50	0.17	-	15.25	12.88	14.06
5	48.94	49.3	1.9	0.74	4.73	-	-	0.06	-	5.44	-	-

SD - standard deviation of the experimental results

$[10^o]_T$ - measured by longitudinal tension testing of an 10^o fabric reinforced laminate

$[\pm 45^o]_T$ - measured by longitudinal tension testing of an $\pm 45^o$ fabric reinforced laminate

SG - measured by the strain gage method

DM - measured by the dilatometer method

the weaving process, being possible in this way to wisely select them to meet both the manufacturing and performance requirements of the composite material. For example, a certain amount of gap between tows improves the ability of fabric to conform to complex mold shapes and also has an influence on the elastic modulus and the strength of the composite. The outcome of a parametric study about longitudinal elastic modulus is presented in Fig. 6 - 7, where a balanced plain weave reinforcement type was considered ($a_f = a_w, h_f = h_w, g_f = g_w$). While the tow width and the tow fiber volume fraction were kept constant, $a_{f,w} = 2mm, V_f^{f,w} = 0.7$, the influence of the tows thickness $h_{f,w}$ and the gap between tows $g_{f,w}$ on the overall fiber volume fraction V_f^0 and the longitudinal elastic modulus E_x have been analyzed. The $h_{f,w}$ and $g_{f,w}$ parameters have been varied in a range of possible practical values.

It can be concluded from Fig. 6 that the tow thickness $h_{f,w}$ has almost no influence on the overall fiber volume fraction V_f^0, for both low and high values of the gap $g_{f,w}$. However, the high gap level strongly reduces the value of V_f^0 compared to the low gap level.

Regarding the elastic modulus E_x, the thickness $h_{f,w}$ has a considerable influence at low values of the gap, and has a negligible influence at very high gap values (Fig. 6). However, at very high gap values the elastic modulus is strongly reduced compared to low gap values.

It can be seen in Fig. 7 that the gap $g_{f,w}$ has a considerable influence on the overall fiber volume fraction V_f^0 for both high and low values of the tows thickness $h_{f,w}$. The influence of $g_{f,w}$ on the elastic modulus is more accentuated for low values of $h_{f,w}$, and it is diminished for increasing values of $h_{f,w}$.

4 Stress, Failure Analysis, and Strength

As explained in the previous sections, due to the complex 3D structure of the woven fabric reinforcement (variable of-axis angle $\theta_{f,w}(x, y)$ (4), and variable thickness $e_{f,w}(x, y)$ (2) of the stacked fill and warp layers, Fig. 5), a stiffness field (10) is generated over the RVE. This stiffness field will generate, in turn, a strain-stress field over the RVE, under external loading. More than contributing at generating the variability in the local values of the stiffness coefficients, the local undulation angles $\theta_{f,w}(x, y)$ play a role in resolving the resulting stress values from the global coordinate system (x, y, z) in the local (material) coordinate system $(1, 2, 3)$, in order to consider failure initiation and evolution of the composite material. Thus, the complex 3D geometrical structure of the RVE

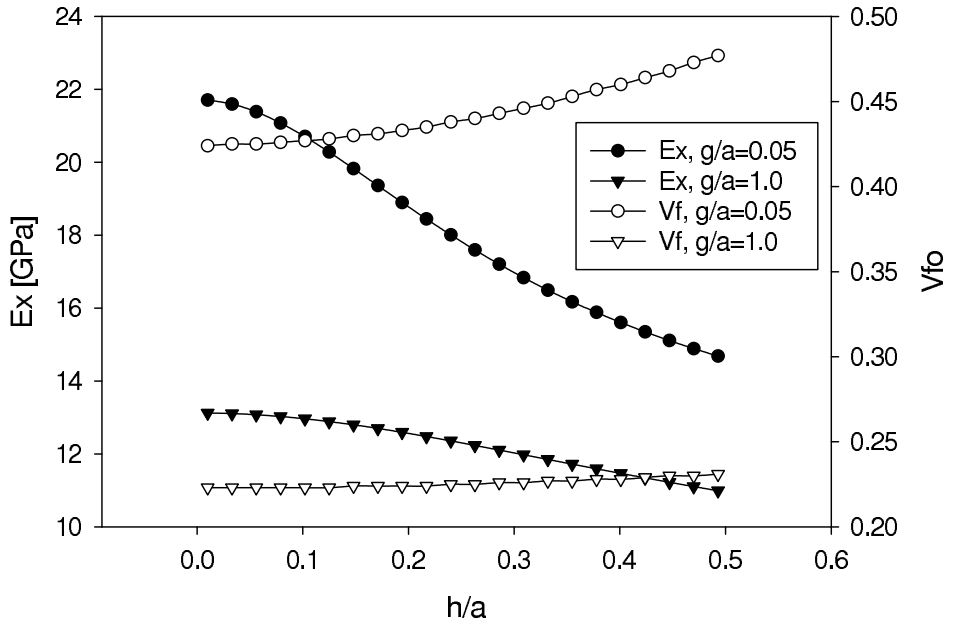

Figure 6: Overall fiber volume fraction V_f^o, and laminate modulus E_x as function of the thickness-to-pitch ratio h/a, for two values of gap-to-pitch ratio g/a.

translates in a complex strain-stress state under external loading, and a complex failure initiation and evolution analysis.

In order to perform this stress and failure analysis, the point-wise CLT is invoked to calculate the resulting strain-stress field. The case of in-plane loading $\{N_x, N_y, N_{xy}\}^T$ is considered here, where the $N_{x,y,xy}$ loading components are considered as uniformly distributed over the RVE width (Fig. 5, 9).

Two different approaches can be considered regarding the constitutive law of the fabric-reinforced composite material. First, taking into account that the stacking sequence matrix/fill/warp/matrix behaves as an asymmetric laminate, the local extension-bending coupling coefficients $B_{i,j}(x,y)$ in (10) are non-zero. This imposes the following local constitutive relationship of CLT for the resulting strain field (called *bending allowed model* [3])

$$\begin{Bmatrix} \varepsilon_{x0} \\ \varepsilon_{y0} \\ \gamma_{xy0} \\ k_x \\ k_y \\ k_{xy} \end{Bmatrix} (x,y) = \begin{bmatrix} [A_{i,j}(x,y)] & [B_{i,j}(x,y)] \\ [B_{i,j}(x,y)] & [D_{i,j}(x,y)] \end{bmatrix}^{-1} \cdot \begin{Bmatrix} N_x \\ N_y \\ N_{xy} \\ M_x \\ M_y \\ M_{xy} \end{Bmatrix} \tag{16}$$

where the $M_{x,y,xy}$ components are zero for the considered case of in-plane loading, but the resulting local curvatures $k_{x,y,xy}$ are non-zero, due to the extension-bending coupling of the asymmetric stacking sequence.

However, it can be shown [1, 22], that for a plain weave pattern, the overall bending effect over the RUC (Fig. 3, 4) is restrained due to the exactly opposite undulations of two adjacent fill/warp tows, this generating exactly opposite local stacking sequences, and opposite signs for the local coupling extension-bending stiffness coefficients in (10). When the homogenization model is used

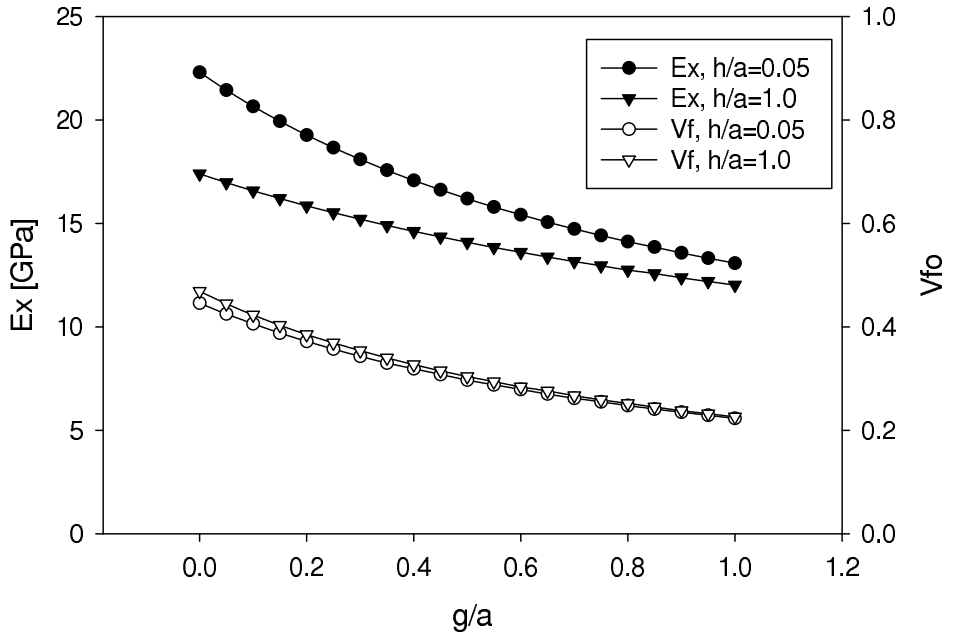

Figure 7: Overall fiber volume fraction V_f^o, and laminate modulus E_x as function of the gap-to-pitch ratio g/a, for two values of thickness-to-pitch ratio h/a.

for calculation of the local stiffness coefficients, the overall bending-extension coupling coefficients becomes zero, and thus the resulting local curvatures field in (16) is restrained to zero.

Another fact that contributes to considering zero curvatures is that the considered RVE does not come from a single ply reinforcement lamina, but it comes from a laminate with multiple plies (as in Fig. 2). This laminates locally behaves as a cross-ply stacking sequence laminate, and it is known from CLT that the induced bending effect is reduced with the increasing number of cross-plies. This allows the use of a simplified constitutive law of the fabric reinforced composite material (called *bending restrained model*)

$$\left\{ \begin{array}{c} \epsilon_x^0(x,y) \\ \epsilon_y^0(x,y) \\ \gamma_{xy}^0(x,y) \end{array} \right\} = [A_{i,j}(x,y)]^{-1} \left\{ \begin{array}{c} N_x \\ N_y \\ N_{xy} \end{array} \right\} \tag{17}$$

where the local mid-plane strains are constant over the RVE thickness. It has to be noted that the bending restrained effect as explained above clearly stands as long as bonding exists between adjacent tows of the fabric reinforced composite in order to globally restrain the locally induced bending; that is, as long as failure does not take place inside of the composite. After failure appears and gradually propagates under the increasing load, it is possible that the bonding is gradually lost, and the bending restrained model may not represent exactly the material behavior. Yet, the bending restrained model has been used in this work and, after failure initiation, the resulting strength predictions agrees with experimental values (Tables 4 - 5).

After calculating the resulting strain field by the constitutive equation (17), the resulting stress field in the fill and warp constituents are calculated according to CLT as

$$\left\{ \begin{array}{c} \sigma_x \\ \sigma_y \\ \sigma_{xy} \end{array} \right\}_{f,w} (x,y) = [\overline{Q}(x,y)]_{f,w} \left\{ \begin{array}{c} \epsilon_x \\ \epsilon_y \\ \gamma_{xy} \end{array} \right\} (x,y) \tag{18}$$

where the local stiffness of the individual fill and warp ply constituents $[\overline{Q}(x,y)]_{f,w}$ is given by (31). Then, the stress components in the global (x,y,z) coordinate system are transformed in the fill and warp local (material) coordinate systems, in order to check the failure initiation and to monitor the failure evolution inside of the RVE

$$\{\sigma_1,\sigma_2,\sigma_3,\sigma_4,\sigma_5,\sigma_6\}^T_{f,w}(x,y)=[T]_{f,w}(x,y)\cdot\{\sigma_x,\sigma_y,0,0,0,\sigma_{xy}\}^T_{f,w}(x,y) \tag{19}$$

where the corresponding fill and warp stress transformation matrices $[T]_{f,w}(x,y)$ are given by (27), (28) (here the superscript T denotes the transpose of the array).

For failure analysis, a *failure initiation criterion* and a *failure evolution criterion* are required in order to detect the conditions for failure onset and progression. Here, the *maximum stress failure criterion* is considered for failure initiation and progression, and a *point-wise stiffness reduction scheme* is considered during failure evolution. Thus, the $I_k, k=1\ldots6$ failure indexes are defined as

$$[I_1,I_2,I_3,I_4,I_5,I_6]^T=[\sigma_1/F_{1t},\sigma_2/F_{2t},\sigma_3/F_{3t},\sigma_4/F_4,\sigma_5/F_5,\sigma_6/F_6]^T \tag{20}$$

where the $F_{1t},F_{2t},F_{3t},F_4,F_5,F_6$ represent the longitudinal tensile and shear strength values of fill/warp tows (considered as unidirectional reinforcements with fiber volume fraction $V_f^{f,w}$ (9)). Based on the I_k indexes, six different failure modes are monitored at any (x,y) location of the RVE, for individual fill and warp constituents:
- *mode1*, $I_1\geq 1$: longitudinal failure, due to tensile stress along 1 direction (fiber direction);
- *mode2*, $I_2\geq 1$: transverse failure, due to tensile stress along 2 direction (perpendicular to fiber direction);
- *mode3*, $I_3\geq 1$: transverse failure, due to tensile stress along the 3 direction (perpendicular to fiber direction);
- *mode4*, $I_4\geq 1$: transverse shear failure, due to shear stress in $2-3$ plane;
- *mode5*, $I_5\geq 1$: transverse shear failure, due to shear stress in $1-3$ plane;
- *mode6*, $I_6\geq 1$: in-plane shear failure, due to shear stress in $1-2$ plane.

In this way, the complex 3D stress state inherent to fabric reinforcements is preserved and monitored. Next, when a local failure is detected ($I_k\geq 1$) under increasing external loading, the stiffness coefficient corresponding to the detected mode of failure, for the corresponding fill/warp/matrix constituent, at the corresponding (x,y) location inside of the RVE, is degraded by a degradation factor $d_i^{f,w}, i=1\ldots3$.

A second-order *damage tensor* $\mathbf{D^{f,w}}$ is defined in material coordinate system as $D_{ij}^{f,w}=d_i^{f,w}\cdot\delta_{ij}$ $(i,j=1\ldots3$, no sum on $i)$ [17] in order to represent damage in individual fill and warp components. The corresponding second order *integrity tensor* is $\mathbf{\Omega^{f,w}}=\sqrt{\mathbf{I}-\mathbf{D^{f,w}}}$ (where $\mathbf{I}$ is the 3×3 unit matrix), and the *material damaged stiffness tensor* can be written in contracted matrix form as [17]

$$C_d^{f,w}=\begin{bmatrix} C_{11}\Omega_1^4 & C_{12}\Omega_1^2\Omega_2^2 & C_{13}\Omega_1^2\Omega_3^2 & 0 & 0 & 0\\ C_{12}\Omega_1^2\Omega_2^2 & C_{22}\Omega_2^4 & C_{23}\Omega_2^2\Omega_3^2 & 0 & 0 & 0\\ C_{13}\Omega_1^2\Omega_3^2 & C_{23}\Omega_2^2\Omega_3^2 & C_{33}\Omega_3^4 & 0 & 0 & 0\\ 0 & 0 & 0 & C_{44}\Omega_2^2\Omega_3^2 & 0 & 0\\ 0 & 0 & 0 & 0 & C_{55}\Omega_1^2\Omega_3^2 & 0\\ 0 & 0 & 0 & 0 & 0 & C_{66}\Omega_1^2\Omega_2^2 \end{bmatrix} \tag{21}$$

where the stiffness coefficients $C_{i,j}$ in (21) are defined in fill/warp $(1,2,3)$ material coordinate system, and the stiffness matrix in (21) is the inverse of the compliance matrix in (24), $[C]=[S]^{-1}$.

When local failure is detected in one of the fill/warp constituents according with (20), the local stiffness of the corresponding fill/warp constituent is degraded according with (21). The following set of stiffness degradation factors $d_i^{f,w}$ has been used in this work:

- for *mode 1*: $d_1 = 0.99, d_2 = d_3 = 0$
- for *mode 2* and *mode 6*: $d_1 = 0, d_2 = 0.9, d_3 = 0$
- for *mode 3* and *mode 5*: $d_1 = d_2 = 0, d_3 = 0.9$
- for *mode 4*: $d_1 = 0, d_2 = d_3 = 0.9$

It is possible that at high values of applied load, some of the above modes of failure simultaneously take place at the same location; in this case, track of the encountered failure modes is kept, and the corresponding damage tensors $\mathbf{D^{f,w}}$ are superposed. With regard to the failure inside of the pure matrix layer (which is isotropic) at a given location, the von Misses failure criterion is used as failure criterion, and an isotropic value of the stiffness degradation factor $d = 0.99$ is used once damage is detected. The components d, d_1, d_2, d_3, can be chosen by the analyst based on experience and thus allowing for adjusting the model to particular material behavior. When the neat matrix fails and when a tow fails along the fiber direction (mode 1), the failed element is likely to loose all it's strength and thus $d = 0.99, d_1 = 0.99$, are chosen, respectively. On the other hand, when a tow damages transversely (mode 2), in in-plane shear (mode 6), and transverse shear (modes 4,5), it is always constrained by surrounding fibers from the other tows, so it is unlikely that the damaged element looses all of its load carrying capacity, thus $d = 0.9$ is chosen for the analysis.

Unlike for the stiffness calculation (Section 3) where the local point-wise stiffness values are integrated over the RVE domain, the stiffness degradation approach for the damage evolution is different, because it is not possible to degrade a point. Instead, regions of material expected to undergo stiffness degradation of fill/warp/matrix constituents are defined, by defining a surface mesh which goes trough the RVE thickness, as show in Fig. 5. In this way, (i, j) elements (where $i, j = 1..n$) of matrix/fill/warp/matrix stacking sequence are monitored for damage modes in any of the fill/warp/matrix constituents. The stress calculation is performed in the central (x, y) point of the (i, j) element, and once damage is detected in one constituent at that central location, the stiffness is degraded for that constituent of the (i, j) element. The damage evolution is approached in this discrete manner, and a convergence study implemented to determine the required number of elements n to be used to discretize the RVE.

Next, the overall (composite material) stiffness matrix in (12) is updated while the damage is evolving under the increasing loading. The overall strains are calculated as

$$\{\epsilon_{x0}, \epsilon_{y0}, \gamma_{xy0}\}^T = [A_{i,j}]^{-1} \cdot \{N_x, N_y, N_{xy}\}^T \tag{22}$$

and the overall stresses are calculated as

$$\{\sigma_x, \sigma_y, \sigma_{xy}\}^T = \{N_x/h, N_y/h, N_{xy}/h\}^T \tag{23}$$

The stress-strain relationship can be evaluated before damage initiation (when the stiffness degradation factors are zero), and after damage initiation (when the stiffness degradation factors are assigned their values according to the detected modes of failure), in order to construct the stress-strain material curves up to final failure, as shown in Fig. 8.

Additional modeling features are implemented in order to simulate the stress redistribution from damaged to undamaged constituents (fill/warp/matrix), and from damaged to undamaged (i, j) elements during damage evolution.

First, *local stress redistribution* is implemented. When a certain mode of failure is encountered in one phase (fill/warp/matrix constituent) of a given (i, j) element, and the corresponding stiffness

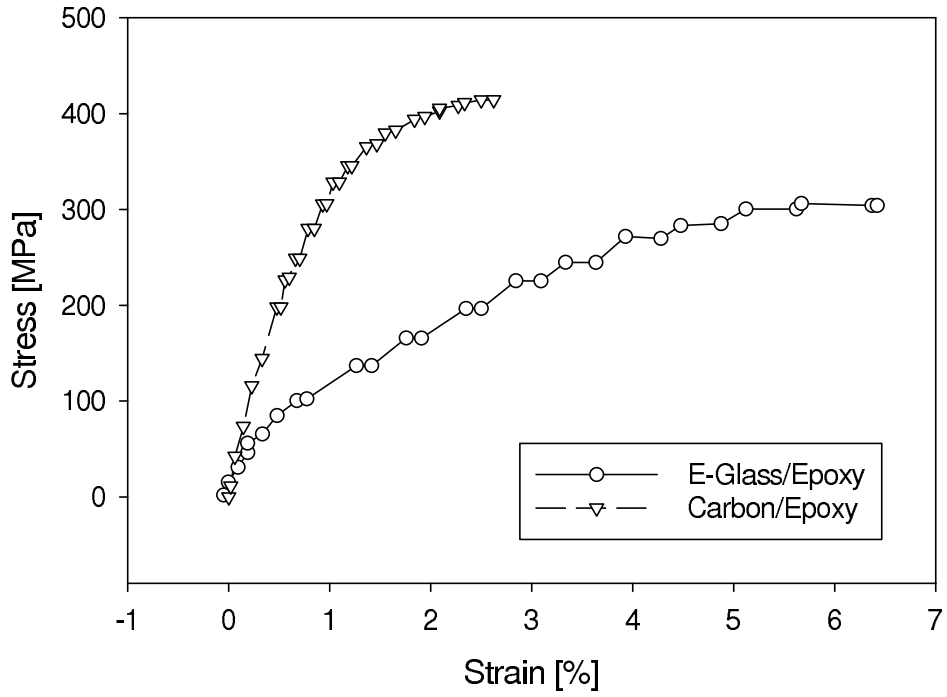

Figure 8: Stress-strain plot for $N_x \neq 0, N_y = N_{xy} = 0$ loading case. (a) E-Glass/Epoxy sample #2 in Table 1; (b) Carbon/Epoxy sample #5 in Table 1.

coefficients are accordingly degraded, that constituent is no longer able to carry load along the degraded direction. The stresses from the damaged constituent are redistributed to the undamaged constituents, at the same level of the external loading ($\sigma_{f1} > \sigma_f$ and $\sigma_{m1} > \sigma_m$ in the case of warp damage longitudinal loading N_x).

Second, *global load redistribution* over the RVE is implemented for the case of longitudinal loading N_x, N_y (Fig. 9). When the longitudinal fiber failure is encountered in a constituent of a given (i, j) element (noted as *(a) = failed and degraded* in Fig. 9), it is assumed that the longitudinal load carrying capacity is also lost for all the elements (noted as *(b) = not failed but degraded* in Fig. 9) in the same line with the failed element along the direction of the applied longitudinal load. This loss of load carrying capacity of elements along the fiber direction is due to the periodicity of the RVE, which implies periodicity of failure along the direction of longitudinal load, and the inability of material to recover the longitudinal stress by shear lag. In this case, the applied load is redistributed over the remaining cells (noted *(c) = not failed, not degraded* in Fig. 9) of the RVE where longitudinal fiber failure has not taken place yet. This load redistribution happens at the same level of the external loading N_x, and it is proportional with the length ω of the degraded element: $N_{x1} = N_x \frac{L}{L_1} > N_x$ in Fig. 9.

The final failure, and accordingly the strength value, is found when all elements are degraded along the direction of loading. The predicted strength values in the cases of longitudinal and shear loading, and the comparison versus experimental results [8] are presented in Table 4. Prediction of laminate ultimate strength is a very difficult task. The model compares reasonably well with errors between 5 and 15% for tensile strength. Prediction of shear strength is even more difficult due to the difficulty in obtaining a uniform state of shear in the experiment and shear nonlinearity. However, the model compares reasonably well, with errors between 2.6 and 11.7% when compared to experimental data obtained with ASTM D5379. The other two type of shear testing methods,

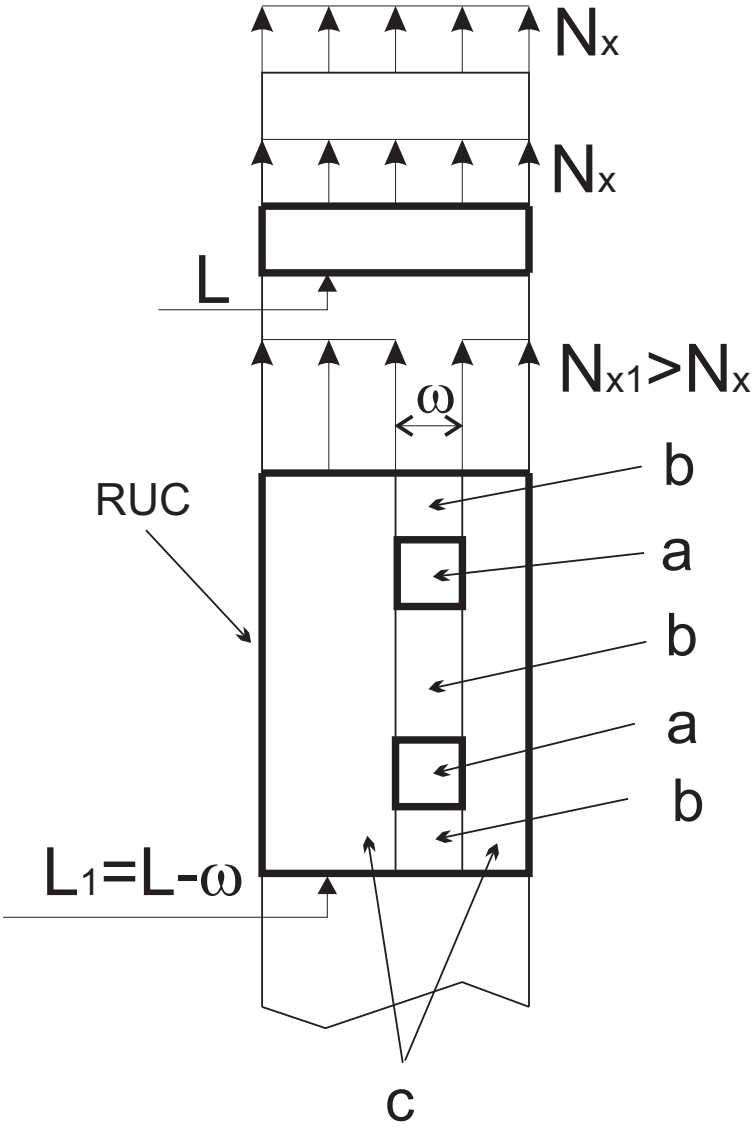

Figure 9: Load redistribution as a result of longitudinal fill failure in one element.

namely 10^o test and ± 45 test to measure shear strength by performing a tensile test are notoriously less accurate, thus the reported data does not compare well with the experimental data obtained with ASTM D5379 or with the model predictions.

Lastly, it is common practice to evaluate the material properties of fabric reinforced composites by approximating the woven reinforced composite with an equivalent cross-ply laminate, at the same overall fiber volume fraction V_f^0. This method is used due to its expedience, and/or due to lack of an adequate model dedicated to woven type reinforcements. It can be seen in Table 5 that the equivalent cross-ply method is far from providing satisfactory results. Therefore, a dedicated model which takes into account all the complex features of the woven reinforcement is necessary.

Table 4: Comparison between predicted and experimental [8] strength values.

Fabric	F_{xt} [MPa]		[%]		F_{xy} [MPa]			
sample	Calc.	Exp.	SD	error	Calc.	Exp. D5379	Exp. $[10^o]_T$	Exp. $[\pm 45^o]_T$
1	275	262	21.0	4.96	36	33	28	26
2	310	318	5.9	2.52	38	34	27	24
3	335	320	6.2	4.69	38	-	-	-
4	325	367	8.0	11.44	38	39	30	26
5	415	490	13.2	15.31	106	-	-	-

D5379 - measured by Iosipescu test method ASTM D5379

$[10^o]_T$ - measured by longitudinal tension testing of an 10^o fabric reinforced laminate

$[\pm 45^o]_T$ - measured by longitudinal tension testing of an $\pm 45^o$ fabric reinforced laminate

Table 5: Comparison between the woven fabric model and the cross-ply symmetric laminate model, strength values.

	V_f^o [%]	F_{xt} [MPa] calculated			F_{xt} [MPa] experimental	error [%]	
#		UD	CP	woven	woven	CP	woven
1	0.32	533	268	275	262	2.1	4.9
2	0.40	855	428	310	318	34.4	2.5
3	0.43	913	458	335	320	43.0	4.7
4	0.46	970	485	325	367	32.1	11.4
5	0.44	1110	555	415	490	13.3	15.3

5 Conclusions

The model predicts well the available experimental data including data for longitudinal, transverse and shear moduli, Poisson's ratio, coefficients of thermal expansion, as well as tensile and shear strength. Also, the model has the ability to predict the coefficients of moisture expansion and can be easily extended to predict strength values under general, combined states of in-plane loads. The equivalent cross-ply laminate analysis method is shown to be significantly less accurate than the proposed model. The present model achieves accuracy in modeling the complexity of geometry and material behavior with a relatively simple formulation, which opens the possibility for further development, for example, to combined in-plane loading cases, or to approach other more complicated weaving styles such as twill and satin reinforcements. Also the proposed geometrical description proved to be accurate enough to produce accurate predictions while simple enough to be used in a general model with gap between individual tows. The parametric study illustrates the effect of gap (g/a) and crimp (h/a) on overall fiber volume fraction (V_f^0) and elastic modulus (E_x). Similar studies can be easily conducted to evaluate other response parameters.

Appendix: Mechanical Properties of Individual Tows

The classical theory [17, 19] is used to calculate the local properties of fill and warp tows, which are rotated at angles $\theta_{f,w}(x,y)$ (4) about the x and y axes of the global coordinate system (x,y,z) (Fig. 3 and 5).

The tow properties of fill and warp in $(1,2,3)$ material c.s. are calculated at tow fiber volume fraction $V_f^{f,w}$ (9), using micromechanical models. Thus, the compliance matrix of will/warp in material c.s. is

$$S = \begin{bmatrix} 1/E_{11} & -\nu_{21}/E_{22} & -\nu_{31}/E_{33} & 0 & 0 & 0 \\ -\nu_{12}/E_{11} & 1/E_{22} & -\nu_{32}/E_{33} & 0 & 0 & 0 \\ -\nu_{13}/E_{11} & -\nu_{23}/E_{22} & 1/E_{33} & 0 & 0 & 0 \\ 0 & 0 & 0 & 1/G_{23} & 0 & 0 \\ 0 & 0 & 0 & 0 & 1/G_{13} & 0 \\ 0 & 0 & 0 & 0 & 0 & 1/G_{12} \end{bmatrix} \tag{24}$$

The rotation matrix from global (x,y,z) to local $(1,2,3)$ c.s (Fig. 5) is expressed as

$$\Omega_f(x), \Omega_w(y) = \begin{bmatrix} {}^c l_1 & {}^c m_1 & {}^c n_1 \\ {}^c l_2 & {}^c m_2 & {}^c n_2 \\ {}^c l_3 & {}^c m_3 & {}^c n_3 \end{bmatrix} \tag{25}$$

where l, m, n are the direction cosines of the coordinate system rotation, and c represents the fill and warp constituent. The stress transformation matrix from global to local c.s is then written as

$$T_f(x), T_w(y) = \begin{bmatrix} {}^c l_1^2 & {}^c m_1^2 & {}^c n_1^2 & 2\,{}^c m_1\,{}^c n_1 & 2\,{}^c l_1\,{}^c n_1 & 2\,{}^c l_1\,{}^c m_1 \\ {}^c l_2^2 & {}^c m_2^2 & {}^c n_2^2 & 2\,{}^c m_2\,{}^c n_2 & 2\,{}^c l_2\,{}^c n_2 & 2\,{}^c l_2\,{}^c m_2 \\ {}^c l_3^2 & {}^c m_3^2 & {}^c n_3^2 & 2\,{}^c m_3\,{}^c n_3 & 2\,{}^c l_3\,{}^c n_3 & 2\,{}^c l_3\,{}^c m_3 \\ {}^c l_2\,{}^c l_3 & {}^c m_2\,{}^c m_3 & {}^c n_2\,{}^c n_3 & {}^c m_2\,{}^c n_3 +{}^c n_2\,{}^c m_3 & {}^c l_2\,{}^c n_3 +{}^c n_2\,{}^c l_3 & {}^c l_2\,{}^c m_3 +{}^c m_2\,{}^c l_3 \\ {}^c l_1\,{}^c l_3 & {}^c m_1\,{}^c m_3 & {}^c n_1\,{}^c n_3 & {}^c m_1\,{}^c n_3 +{}^c n_1\,{}^c m_3 & {}^c l_1\,{}^c n_3 +{}^c n_1\,{}^c l_3 & {}^c l_1\,{}^c m_3 +{}^c m_1\,{}^c l_3 \\ {}^c l_1\,{}^c l_2 & {}^c m_1\,{}^c m_2 & {}^c n_1\,{}^c n_2 & {}^c m_1\,{}^c n_2 +{}^c n_1\,{}^c m_2 & {}^c l_1\,{}^c n_2 +{}^c n_1\,{}^c l_2 & {}^c l_1\,{}^c m_2 +{}^c m_1\,{}^c l_2 \end{bmatrix} \tag{26}$$

which after calculations takes the simplified form for individual fill and warp tows

$$T_f(x) = \begin{bmatrix} c_f^2 & 0 & s_f^2 & 0 & 2c_f s_f & 0 \\ 0 & 1 & 0 & 0 & 0 & 0 \\ s_f^2 & 0 & c_f^2 & 0 & -2c_f s_f & 0 \\ 0 & 0 & 0 & c_f & 0 & -s_f \\ -c_f s_f & 0 & c_f s_f & 0 & c_f^2 - s_f^2 & 0 \\ 0 & 0 & 0 & s_f & 0 & c_f \end{bmatrix} \tag{27}$$

and

$$T_w(y) = \begin{bmatrix} 0 & c_w^2 & s_w^2 & -2c_w s_w & 0 & 0 \\ 1 & 0 & 0 & 0 & 0 & 0 \\ 0 & s_w^2 & c_w^2 & 2c_w s_w & 0 & 0 \\ 0 & 0 & 0 & 0 & -c_w & -s_w \\ 0 & c_w s_w & -c_w s_w & c_w^2 - s_w^2 & 0 & 0 \\ 0 & 0 & 0 & 0 & s_w & -c_w \end{bmatrix} \tag{28}$$

where

$$\begin{aligned} s_f(x) &= sin\ \theta_f(x) \\ c_f(x) &= cos\ \theta_f(x) \\ s_w(y) &= sin\ \theta_w(y) \\ c_w(y) &= cos\ \theta_w(y) \end{aligned} \tag{29}$$

The 3D compliance matrix of fill and warp constituents written in laminate (x, y, z) c.s. becomes

$$\begin{aligned} \overline{S}_f(x) &= [T_f(x)]^T \cdot S \cdot T_f(x) \\ \overline{S}_w(y) &= [T_w(y)]^T \cdot S \cdot T_w(y) \end{aligned} \tag{30}$$

where $[S]$ is given by (24).

Considering the plane stress state in the (x, y) plane of the laminate, the corresponding $(i, j) = 1, 2, 6$ terms are selected from (30), and the reduced fill and warp local stiffness matrices can be expressed in the global coordinate system (x, y, z), at any given location (x, y) as

$${}^c\overline{Q} = \begin{bmatrix} {}^c\overline{Q}_{11} & {}^c\overline{Q}_{12} & 0 \\ {}^c\overline{Q}_{21} & {}^c\overline{Q}_{22} & 0 \\ 0 & 0 & {}^c\overline{Q}_{66} \end{bmatrix} = \begin{bmatrix} {}^c\overline{S}_{11} & {}^c\overline{S}_{12} & 0 \\ {}^c\overline{S}_{21} & {}^c\overline{S}_{22} & 0 \\ 0 & 0 & \overline{S}_{66} \end{bmatrix}^{-1} \tag{31}$$

where c represents the fill or warp constituent.

The classical approach [17,19] is followed for calculation of the thermal and moisture expansion

coefficients,

$$\left\{\begin{array}{c}\alpha_x\\ \alpha_y\\ \alpha_z\\ \frac{1}{2}\alpha_{yz}\\ \frac{1}{2}\alpha_{xz}\\ \frac{1}{2}\alpha_{xy}\end{array}\right\}_{f,w}(x,y)=[T]^{-1}_{f,w}(x,y)\left\{\begin{array}{c}\alpha_1\\ \alpha_2\\ \alpha_3\\ 0\\ 0\\ 0\end{array}\right\}_{f,w}\qquad \left\{\begin{array}{c}\beta_x\\ \beta_y\\ \beta_z\\ \frac{1}{2}\beta_{yz}\\ \frac{1}{2}\beta_{xz}\\ \frac{1}{2}\beta_{xy}\end{array}\right\}_{f,w}(x,y)=[T]^{-1}_{f,w}(x,y)\left\{\begin{array}{c}\beta_1\\ \beta_2\\ \beta_3\\ 0\\ 0\\ 0\end{array}\right\}_{f,w} \tag{32}$$

and the in-plane terms of interest are selected from 32 as

$$\begin{array}{lll}\alpha_{xf}(x)=\alpha_1c_f^2+\alpha_2s_f^2 & \alpha_{yf}(x)=\alpha_2 & \alpha_{xyf}=0\\ \alpha_{xw}(y)=\alpha_2 & \alpha_{yw}(y)=\alpha_1c_w^2+\alpha_2s_w^2 & \alpha_{xyw}=0\\ \beta_{xf}(x)=\beta_1c_f^2+\beta_2s_f^2 & \beta_{yf}(x)=\beta_2 & \beta_{xyf}=0\\ \beta_{xw}(y)=\beta_2 & \beta_{yw}(y)=\beta_1c_w^2+\beta_2s_w^2 & \beta_{xyw}=0\end{array} \tag{33}$$

The above transformation can be easily computed when noted that $[T]^{-1}_{f,w}=[\overline{T}]^T_{f,w}$, where $[\overline{T}]=[R][T][R]^{-1}$, $[R]$ is the Reuter matrix ($R_{ij}=1$ for $i=j=1\ldots3$, $R_{ij}=2$ for $i=j=4\ldots6$, and $R_{ij}=0$ for $i\neq j$).

It has to be noted that the coefficients $(i,j)=3,4,5$ may be different from zero in (30). By selecting only the in-plane terms $(i,j)=1,2,6$ in (31), the coupling effects associated to $(i,j)=3,4,5$ are neglected.

References

[1] Tsu-Wei Chou, (1992) Microstructural Design of Fiber Composites, Cambridge University Press, Cambridge

[2] Makoto Ito, Tsu Chou, (1997) 'Elastic Moduli and Stress Field of Plain Weave Composites Under Tensile Loading', Composites Science and Technology, 57, 787-800

[3] Makoto Ito, Tsu Chou, (1998) 'An Analytical and Experimental Study of Strength and Failure Behavior of Plain Weave Composites', Journal of Composite Materials, 32(1), 2-30

[4] D. Scida, Z. Aboura, (1997) 'Prediction of the Elastic Behavior of Hybrid and non-Hybrid Woven Composites', Composite Science and Technology, 59, 1727-1740

[5] D. Scida, Z. Aboura, (1999) 'A micromechanics model for 3D elasticity and failure of woven fiber composite materials', Composite Science and Technology, 59, 505-517

[6] N. Naik, V. Ganesh, (1992) 'Prediction of On-Axis Elastic Properties of Plain Weave Fabric Composites', Composite Science and Technology, 45, 135-152

[7] N. Naik, V. Ganesh, (1996) 'Failure Behavior of Plain Weave Fabric Laminates Under On-Axis Uniaxial Tensile Loading: I - Laminate Geometry', Journal of Composite Materials, 30(16), 1748-1778

[8] N. Naik, V. Ganesh, (1996) 'Failure Behavior of Plain Weave Fabric Laminates Under On-Axis Uniaxial Tensile Loading: II - Analytical Predictions', Journal of Composite Materials, 30(16), 1779-1882

[9] N. Naik, V. Ganesh, (1996) 'Failure Behavior of Plain Weave Fabric Laminates Under On-Axis Uniaxial Tensile Loading: III - Effect of Fabric Geometry', Journal of Composite Materials, 30(16), 1883-1856

[10] Adi Adumitroaie, Ever J. Barbero, (2011) 'Beyond plain weave fabrics - I. Geometrical model', Composite Structures, 93, 1424-32

[11] Adi Adumitroaie, Ever J. Barbero, (2011) 'Beyond plain weave fabrics - II. Mechanical properties', Composite Structures, 93, 1449-62

[12] N. Naik, V. Ganesh, (1997) 'Thermo-Mechanical Behavior of Plain Weave Fabric Composites: Experimental Investigations', Journal of Materials Science, 32, 267-277

[13] ASTM D3171 Standard Test Methods for Constituent Content of Composite Materials, vol. 15.03, ASTM International, West Conshohocken, PA, 19428-2959 USA.

[14] ASTM D2584 Standard Test Method for IGNITION LOSS of Cured Reinforced Resins, vol. 08.01, ASTM International, West Conshohocken, PA, 19428-2959 USA.

[15] J. Falzon, I. Herszberg, (1996) 'Effects of Compaction on the Stiffness and Strength of Plain Weave Fabric RTM Composites', Journal of Composite Materials, 30(11), 1210-1247

[16] Barbero, E. J.; Trovillion, J.; Mayugo, J.A.; Sikkil, K.K. (2006) 'Finite element modeling of plain weave fabrics from photomicrograph measurements', Composite Structures, v 73, n 1, p 41-52.

[17] Barbero, E. J. (2007) Finite Element Analysis of Composite Materials, CRC Press, Boca Raton, FL.

[18] R. Luciano, E. J. Barbero (1995) 'Formulas for the Stiffness of Composites with Periodic Microstructure', Int. J. of Solids Structures, 31(21), 2933-2944.

[19] Barbero, E. J. (2010) Introduction to Composite Material Design, 2nd Edition, Taylor & Francis, Boca Raton, FL.

[20] John W. Weeton, Dean M. Peters, Karyn L. Thomas, (1986) Engineer's Guide to Composite Materials, American Soicety for Metals, , Ohio

[21] Kuno K. Stellbrink, (1996) Micromechanics of Composites, Hanser Publishers, Munich Vienna New York, N.Y.

[22] Niranjan K. Naik, (1994) Woven Fabric Composites, Technomic Publishing Co., Lancaster-Basel